Available online at www.sciencedirect.com
SCIENCE DIRECT®
Journal of Computational Physics 189 (2003) 607–625
JOURNAL OF COMPUTATIONAL PHYSICS
www.elsevier.com/locate/jcp

A fast solver for Fokker–Planck equation applied to viscoelastic flows calculations: 2D FENE model

Alexei Lozinski [a,*], Cédric Chauvière [b]

[a] LMF-ISE-FSTI, Ecole Polytechnique Fédérale de Lausanne, Lausanne CH-1015, Switzerland
[b] Division of Applied Mathematics, Brown University, Box F, Providence, RI 02912, USA

Received 28 January 2003; received in revised form 24 April 2003; accepted 24 April 2003

Abstract

In this paper, we introduce a new method for solving efficiently the Fokker–Planck equation arising in the simulation of dilute polymeric solutions. For a two-dimensional FENE (Finitely Extensible Nonlinear Elastic) model, the structure of the Fokker–Planck equation is used to design a fast solver. The resulting equations are discretized with a spectral/spectral element method. Application of the method to flow of a FENE fluid past a confined cylinder demonstrates readily the advantages of the proposed scheme over traditional stochastic simulations.

Keywords: FENE dumbbell model; Fokker–Planck equation; Spectral methods

1. Introduction

In this paper, we are concerned with the simulation of flows of dilute polymeric solutions in complex geometries. The polymeric molecules are represented through kinetic theory, in which case the solvent is treated as a viscous continuum which acts on the macromolecules through thermal fluctuations and viscous drag. One of the simplest kinetic theory models represents the polymeric molecules by dumbbells which consist of two beads connected by a spring (see [3]). In this approach, the statistics of the configuration vector $\mathbf{q}$ determining the direction and the elongation of the spring have to be computed. Kinetic theory provides a partial differential equation (the Fokker–Planck (FP) equation [1]) for the probability density $\psi(t, \mathbf{x}, \mathbf{q})$ of $\mathbf{q}$ and an expression for the polymeric extra-stress $\boldsymbol{\tau}$ in the form of the expectation of certain functions of $\mathbf{q}$. One can also obtain an Itô stochastic differential equation for the random process $\mathbf{q}$, which is formally equivalent to the FP equation. For some polymeric models, it is possible to derive a constitutive

* Corresponding author. Tel.: +42-21-693-5312; fax: +42-21-693-5307.
E-mail addresses: alexei.lozinski@epfl.ch (A. Lozinski), cedric@cfm.brown.edu (C. Chauvière).

[1] The FP equation is also known as the diffusion equation in polymeric kinetic theory or the Smoluchowski equation in the theory of Brownian motion.

0021-9991/$ - see front matter
doi:10.1016/S0021-9991(03)00248-1

equation for the extra-stress and therefore bypass the resolution of equations describing the polymer at a microscopic level (the interested reader can find in [22] an extensive review of numerical methods well suited for models with closed-form constitutive equations of differential and integral type). However, such models are usually unable to predict certain complex behaviour of polymeric fluids, such as the hysteresis phenomenon, for example [24].

One is therefore led to construct efficient numerical techniques to simulate models for which no constitutive equation exists. One can start from the stochastic differential equation for $\mathbf{q}$, introduce a large number of pseudo-random vector fields $\mathbf{q}_m$ (typically several thousand or possibly several hundred when variance reduction techniques are used, see [4,5]) and solve for each of them a partial differential equation that can be discretized by finite elements or any other numerical technique (CONNFFESSIT approach, see [20]). All this must be coupled with the momentum and continuity equations for the velocity and pressure. It is easy to see that such a technique is extremely expensive, even in one of its most efficient versions, the Brownian configuration fields method [17].

One can try to alleviate the three main disadvantages of the Brownian configuration fields method, which are large CPU cost, huge memory requirements and the presence of statistical noise in the computed polymeric stress, by solving directly the FP equation for $\psi(t, \mathbf{x}, \mathbf{q})$ instead of the stochastic differential equation for $\mathbf{q}$. This is what we will do in this paper. Note that the method presented here is well suited only for polymeric models having low dimensional configuration space. Indeed, in the case of more complex models like the Rouse chain consisting of $N \geqslant 3$ beads and $N-1$ springs, the probability density should be solved in a high dimensional space $(t, \mathbf{x}, \mathbf{q}_1, \ldots, \mathbf{q}_{N-1})$ instead of $(t, \mathbf{x}, \mathbf{q})$, making the solution of the FP equation hardly tractable.

A review of the literature reveals that very little has been done in order to advocate this approach, mainly due to the lack of efficient numerical techniques to solve the FP equation. Starting with the pioneer work of Warner in 1972 [28], the FP equation was used there to solve the steady-state shearing flow and small-amplitude oscillatory shearing flow of a FENE fluid. It was only 13 years later, in 1985, that Fan [13] improved the original idea of Warner by requiring that the probability density function be smooth at the origin, leading to more accurate results. The dilute multibead-rod model was the model of choice of Fan in 1989 in a series of two papers [14,15]. The second paper is, to our knowledge, the first attempt in the published literature to use the FP equation for flows in complex geometries. Although simplifying assumptions had to be made (convective terms neglected in the FP equation), the computational difficulty at that time must not be underestimated. In a recent work by a group in MIT [1], the start-up of steady shear flow for dilute solutions of rigid rod-like macromolecules was also treated with the FP equation using Daubechies wavelets for the discretization. In [19], this method was used to simulate the dynamics of both the rigid dumbbell model and the Doi model for monodomain liquid crystalline polymers in a complex flow environment (see also [25]). For the numerical simulations of concentrated polymer solutions, the interested reader is referred to the recent paper of Lozinski et al. [18] for the details.

In this paper, we choose the FENE dumbbell model [28] of dilute polymer solutions. No constitutive equation exists for this model. Contrary to [18], we use here an implicit time-marching for the FP equation that enables us to weaken significantly the stability restriction on the time-step. The first version of our method has been presented in a short paper [7]. In the present paper, we use some properties of the FP equation to reduce significantly the computational cost. We restrict ourselves here to planar flows and we assume, for the sake of simplicity, that the dumbbells lie also in the plane of the flow. This is not a physically reasonable assumption a priori, and we use it primarily to illustrate our numerical method, which can be extended to three-dimensional FENE dumbbells in a future work. We note however that using 2D FENE dumbbells does not deteriorate significantly the predictions of the polymer stress in shear flows [7].

The paper is organized as follows. The next section is a brief description on how dilute polymeric liquids may be modelled. Section 3 presents in more detail the stochastic approach and the discretization of the resulting equations. A novel numerical scheme for the FP equation, which leads to a fast solver for this

equation is then presented in Section 4. Then, in Section 5 we demonstrate the efficiency of our numerical scheme by solving the benchmark problem of the flow past a cylinder in a channel and compare our results with more conventional stochastic simulations and the method of [7]. Finally, in Section 6 we state some conclusions.

2. Problem description

We consider a solvent, which is assumed to be incompressible and isothermal, and we restrict ourselves to the case of inertialess flows (zero Reynolds number). For such a fluid, the mass and momentum conservation equations take the form of the Stokes system that can be written as

$$\mathbf{0} = -\nabla p + 2\eta_s \nabla \cdot \varepsilon(\mathbf{u}) + \nabla \cdot \boldsymbol{\tau}, \tag{1}$$

$$\nabla \cdot \mathbf{u} = 0, \tag{2}$$

where $\mathbf{u}$ denotes the fluid velocity, p is the pressure, $\boldsymbol{\tau}$ is the polymeric contribution to the Cauchy stress tensor, $\varepsilon(\mathbf{u}) = \frac{1}{2}(\nabla \mathbf{u} + \nabla \mathbf{u}^{\mathrm{T}})$ is the rate-of-strain tensor and η_s is the solvent viscosity.

In this paper, we follow the simplest micro-mechanical approach to model the polymer molecules in a dilute solution (the dumbbell model), in which the polymers are represented by two beads connected by a spring (see Fig. 1) and the configuration vector $\mathbf{q}(t)$ describes the orientation and the elongation of such a dumbbell as it moves along its trajectory $\mathbf{x}(t)$. The force of the spring is governed by some law that should be derived from physical arguments. We choose here the popular FENE model, in which the maximum extensibility of the dumbbell is fixed at some value determined by the dimensionless parameter b and the spring force, after some scaling, takes the simple form

$$\mathbf{F}(\mathbf{q}) = \frac{\mathbf{q}}{1 - (|\mathbf{q}|^2/b)}, \tag{3}$$

where both $\mathbf{F}$ and $\mathbf{q}$ are dimensionless vectors.

The configuration vector $\mathbf{q}(t, \mathbf{x})$ of a dumbbell located at $\mathbf{x}$ at time t satisfies the following stochastic differential equation (see [20] for details):

$$\mathrm{d}\mathbf{q}(\mathbf{x}, t) + \mathbf{u}(\mathbf{x}, t) \cdot \nabla \mathbf{q}(\mathbf{x}, t)\mathrm{d}t = \left(\nabla \mathbf{u}(\mathbf{x}, t) \cdot \mathbf{q}(\mathbf{x}, t) - \frac{1}{2\lambda} \mathbf{F}(\mathbf{q}(\mathbf{x}, t)) \right) \mathrm{d}t + \sqrt{\frac{1}{\lambda}} \mathrm{d}\mathbf{W}(\mathbf{x}, t), \tag{4}$$

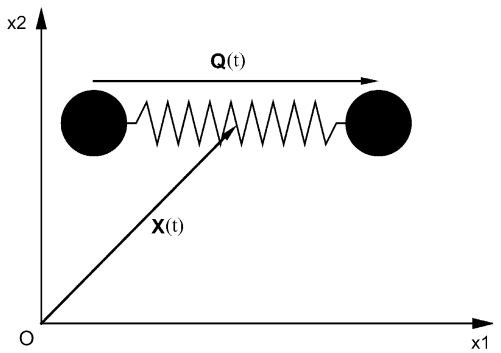

Fig. 1. Description of a single dumbbell placed in the fluid in $\mathbf{X}(t)$.

where $(\nabla \mathbf{u})_{ij} = \partial u_i/\partial x_j$, λ is the relaxation time of the fluid, $\mathbf{W}(\mathbf{x}, t)$ is the Wiener random process that accounts for the Brownian forces acting on each bead. Eq. (4) should be understood as the Itô ordinary stochastic differential equations along the particle paths since the dumbbells' centres of mass are supposed to follow the particles of the solvent fluid.

Alternatively, one can describe the dynamics of polymers in terms of the probability density function (pdf) $\psi(t, \mathbf{x}, \mathbf{q})$ of the random process $\mathbf{q}(t, \mathbf{x})$ that can be interpreted as follows: $\psi(t, \mathbf{x}, \mathbf{q})\mathrm{d}\mathbf{q}$ is the probability that a dumbbell at position $\mathbf{x}$ and at time t is to be found with the configuration vector in the box $[\mathbf{q}, \mathbf{q} + \mathrm{d}\mathbf{q}]$. As is well known (see [20, Section 3.3]), every Itô stochastic differential equation can be associated with the partial differential equation (the FP equation) for the pdf. In particular, Eq. (4) of the FENE dumbbell model, implies the following FP equation for $\psi(t, \mathbf{x}, \mathbf{q})$

$$\frac{\partial \psi}{\partial t} + \mathbf{u} \cdot \nabla \psi + \nabla_{\mathbf{q}} \cdot \left(\left(\nabla \mathbf{u} \cdot \mathbf{q} - \frac{1}{2\lambda} \mathbf{F}(\mathbf{q}) \right) \psi \right) = \frac{1}{2\lambda} \Delta_{\mathbf{q}} \psi, \tag{5}$$

where we use the subscript $\mathbf{q}$ for operators acting in configuration space and no subscript for operators acting in physical space.

Once the statistical information about the distribution of $\mathbf{q}$ is known, the extra-stress tensor $\boldsymbol{\tau}(t, \mathbf{x})$ (which is used in the source term of the momentum equation (1)) can be computed by the *Kramers expression* (see [3, p. 69])

$$\boldsymbol{\tau}(\mathbf{x}, t) = \frac{\eta_{\mathrm{p}}}{\lambda} \frac{b+4}{b} (-\mathbf{I} + \mathbb{E}(\mathbf{q}(\mathbf{x}, t) \otimes \mathbf{F}(\mathbf{q}(\mathbf{x}, t)))), \tag{6}$$

where the symbol $\otimes$ denotes the tensor product of two vectors and $\mathbb{E}(\cdot)$ is the expectation. The prefactor in (6) is chosen so that the viscosity in the linear regime (low shear rates) is equal to $\eta_{\mathrm{s}} + \eta_{\mathrm{p}}$ (for the $2D$ case). The parameter η_{p} is referred to as the zero shear-rate polymeric viscosity.

The two different (although formally equivalent) approaches described above lead to different numerical methods. We shall present stochastic numerical simulations based on Eq. (4) in the following section. Section 4 will be devoted to the direct solution of the FP Eq. (5). Note that in both cases, the velocity gradient is calculated at each time-step and at every grid point from the latest known velocity obtained as a solution to (1) and (2), so we can suppose in the sequel that the velocity field and its gradient are given.

3. Stochastic simulation (Brownian configuration field method)

3.1. Discretization of the stochastic equation

Denoting the discrete times $\mathrm{i}\Delta t$ by t_i, the properties of the Wiener process (see [16], for example) imply $\mathbf{W}(t_0) = \mathbf{0}$ and

$$\mathbf{W}(t_i) = \mathbf{W}(t_{i-1}) + \sqrt{\Delta t} \Delta \mathbf{W}(t_i), \tag{7}$$

where $\Delta \mathbf{W}(t_i)$ are mutually independent random vectors having probability distribution $\mathbf{N}(0, 1)$.

Using a simple backward Euler scheme for the time discretization of (4), we obtain the following stochastic partial differential equation:

$$\frac{\mathbf{q}(\mathbf{x}, t_{i+1}) - \mathbf{q}(\mathbf{x}, t_i)}{\Delta t} + \mathbf{u}(\mathbf{x}, t_i) \cdot \nabla \mathbf{q}(\mathbf{x}, t_{i+1}) - \nabla \mathbf{u}(\mathbf{x}, t_i) \mathbf{q}(\mathbf{x}, t_{i+1}) + \frac{1}{2\lambda} \mathbf{F}(\mathbf{q}(\mathbf{x}, t_i)) = \sqrt{\frac{1}{\lambda \Delta t}} \Delta \mathbf{W}(t_i). \tag{8}$$

Note that the increments of the discrete Wiener process in (8) do not depend on $\mathbf{x}$ although the original stochastic differential equation (4) assumes an independent Wiener process on each particle path. We can afford this simplification since we are interested only in some averages of random vectors $\mathbf{q}(\mathbf{x}, t_i)$. This idea is the basis of the Brownian configuration field method proposed in [17] (see also [27]), and it allows us to reduce drastically the computational cost as well as the random noise in averaged quantities like the extra-stress.

When a Monte-Carlo approach is used for solving (8) a large number of pseudo-random vectors $\{\Delta\mathbf{W}_m(t_i)\}_{1\leqslant m\leqslant M}$ are generated and Eq. (8) has to be solved M times to compute the realizations of $\mathbf{q}$ (also known as configuration fields) $\{\mathbf{q}_m(\mathbf{x}, t_{i+1})\}_{1\leqslant m\leqslant M}$ for each $\Delta\mathbf{W}_m(t_i)$ at the right-hand side. Note that the vectors $\Delta\mathbf{W}_m(t_i)$ are mutually independent in time, therefore a new set of pseudo-random numbers needs to be generated at each time-step. Initially, the fluid is at rest so that the equilibrium extra-stress tensor must be zero. This is done by generating M initial pseudo-random vectors with the following distribution (for the 2D case):

$$\psi_{\mathrm{eq}}(\mathbf{q}) = \frac{b+2}{2\pi b}\left(1 - \frac{|\mathbf{q}|^2}{b}\right)^{b/2}. \tag{9}$$

To prevent the norm of the vectors $\mathbf{q}_m$ from exceeding $\sqrt{b}$ that can result in divergence of the scheme, one can either use rejections techniques or treat the $\mathbf{F}(\mathbf{q})$ term in an implicit way (see [20, Section 4.3.2]). We implement this latter idea using a time splitting technique for Eq. (8):

$$\frac{\widetilde{\mathbf{q}}_m(\mathbf{x}, t_i) - \mathbf{q}_m(\mathbf{x}, t_{i-1})}{\Delta t} + \mathbf{u}(\mathbf{x}, t_i)\cdot\nabla\widetilde{\mathbf{q}}_m(\mathbf{x}, t_i) = 0, \tag{10}$$

$$\frac{\mathbf{q}_m(\mathbf{x}, t_{i+1}) - \widetilde{\mathbf{q}}_m(\mathbf{x}, t_i)}{\Delta t} + \frac{1}{2\lambda}\mathbf{F}(\mathbf{q}_m(\mathbf{x}, t_{i+1})) = \nabla\mathbf{u}(\mathbf{x}, t_i)\widetilde{\mathbf{q}}_m(\mathbf{x}, t_i) + \sqrt{\frac{1}{\lambda\Delta t}}\Delta\mathbf{W}_m(t_i). \tag{11}$$

The first equation should be solved by a numerical method appropriate for hyperbolic PDEs and (11) can be solved independently at every grid point. To see that this splitting prevents the norm of the vectors $\mathbf{q}_m$ from exceeding $\sqrt{b}$, we rearrange (11) and use (3) to arrive at

$$\left(\frac{1}{\Delta t} + \frac{1}{2\lambda}\frac{1}{1 - (|\mathbf{q}_m(\mathbf{x}, t_{i+1})|^2/b)}\right)\mathbf{q}_m(\mathbf{x}, t_{i+1}) = \mathbf{s}_m(\mathbf{x}, t_i), \tag{12}$$

where

$$\mathbf{s}_m(\mathbf{x}, t_i) = \frac{\widetilde{\mathbf{q}}_m(\mathbf{x}, t_i)}{\Delta t} + \nabla\mathbf{u}(\mathbf{x}, t_i)\widetilde{\mathbf{q}}_m(\mathbf{x}, t_i) + \sqrt{\frac{1}{\lambda\Delta t}}\Delta\mathbf{W}_m(t_i)$$

is a known vector since $\widetilde{\mathbf{q}}_m(\mathbf{x}, t_i)$ has been computed from Eq. (10). We put $s_m = |\mathbf{s}_m(\mathbf{x}, t_i)|$ and $q_m = |\mathbf{q}_m(\mathbf{x}, t_{i+1})|$ and derive from (12) the cubic polynomial equation for q_m

$$q_m^3 - \Delta t s_m q_m^2 - b\left(\frac{\Delta t}{2\lambda} + 1\right)q_m + \Delta t s_m b = 0. \tag{13}$$

This equation can be shown to possess one root that satisfies $0 \leqslant q_m < \sqrt{b}$. Having determined this root, the configuration vector $\mathbf{q}_m(\mathbf{x}, t_{i+1})$ is simply

$$\mathbf{q}_m(\mathbf{x}, t_{i+1}) = \left(\frac{1}{\Delta t} + \frac{1}{2\lambda}\frac{1}{1 - (q_m^2/b)}\right)^{-1}\mathbf{s}_m(\mathbf{x}, t_i). \tag{14}$$

3.2. Computation of the extra-stress

Having computed a large number of realizations $\{\mathbf{q}_m(\mathbf{x},t_i)\}_{1\leqslant m\leqslant M}$ that experience different uncorrelated Wiener processes $\{\mathbf{W}_m(t)\}_{1\leqslant m\leqslant M}$ as described above, we are in position to determine the polymeric extra-stress $\boldsymbol{\tau}$ which will then be used as a source term for Eq. (1). We use a straightforward approximation to (6) that is given by

$$\boldsymbol{\tau}(\mathbf{x},t_i)=\frac{\eta_p}{\lambda}\frac{b+4}{b}\left(-\mathbf{I}+\frac{1}{M}\sum_{m=1}^{M}\mathbf{q}_m(\mathbf{x},t_i)\otimes\mathbf{F}(\mathbf{q}_m(\mathbf{x},t_i))\right). \tag{15}$$

However, computing the extra-stress with (15) will give solutions that converge at a slow rate $O(1/\sqrt{M})$ typical of stochastic simulations. Variance reduction techniques make it possible to reduce the noise level [5]; however, the efficiency of such techniques may be less effective as the Deborah number increases [4]. In the following section, we will see how this can be avoided by considering an approach based on the direct solution of the FP equation (5).

4. Direct simulation (FP equation)

4.1. The basic idea

In this approach, we seek the pdf $\psi(t,\mathbf{x},\mathbf{q})$ by solving (5) directly. But first, we give the main ideas that will be developed in the following sections. For reasons that will be explained later we will use a variable $\alpha(t,\mathbf{x},\mathbf{q})$ instead of $\psi(t,\mathbf{x},\mathbf{q})$. The equation for $\alpha(t,\mathbf{x},\mathbf{q})$ can be formally rewritten as

$$\frac{\partial\alpha}{\partial t}+\mathbf{A}_{\mathbf{x}}\alpha+\frac{\partial u_1}{\partial x_1}\mathbf{B}_{\mathbf{q}}\alpha+\frac{\partial u_1}{\partial x_2}\mathbf{C}_{\mathbf{q}}\alpha+\frac{\partial u_2}{\partial x_1}\mathbf{D}_{\mathbf{q}}\alpha=0, \tag{16}$$

where $\mathbf{A}_{\mathbf{x}}=\mathbf{u}\cdot\nabla$ is a linear operator acting only in physical space whereas $\mathbf{B}_{\mathbf{q}}$, $\mathbf{C}_{\mathbf{q}}$ and $\mathbf{D}_{\mathbf{q}}$ are linear operators acting only in configuration space. Therefore, (16) lends itself to a time splitting, which, for a first order backward Euler method leads to

$$\frac{\widetilde{\alpha}^i-\alpha^i}{\Delta t}+\frac{\partial u_1}{\partial x_1}\mathbf{B}_{\mathbf{q}}\widetilde{\alpha}^i+\frac{\partial u_1}{\partial x_2}\mathbf{C}_{\mathbf{q}}\widetilde{\alpha}^i+\frac{\partial u_2}{\partial x_1}\mathbf{D}_{\mathbf{q}}\widetilde{\alpha}^i=0, \tag{17}$$

$$\frac{\alpha^{i+1}-\widetilde{\alpha}^i}{\Delta t}+\mathbf{A}_{\mathbf{x}}\alpha^{i+1}=0. \tag{18}$$

Doing so, Eq. (17) is first solved in configuration space for the auxiliary variable $\widetilde{\alpha}^i$, separately at every grid point of physical space. It is then injected into Eq. (18), which should be solved in physical space in a similar way to Eq. (10). Although the scheme (17) and (18) can be solved directly as was done in [7], such an approach might be quite expensive for non-trivial geometries. To see that, we note that after discretization and keeping the same notations for the discretized and continuous operators, the discrete solutions of (17) and (18) are, respectively,

$$\widetilde{\alpha}^i=\left(\mathbf{I}+\Delta t\left[\frac{\partial u_1}{\partial x_1}\mathbf{B}_{\mathbf{q}}+\frac{\partial u_1}{\partial x_2}\mathbf{C}_{\mathbf{q}}+\frac{\partial u_2}{\partial x_1}\mathbf{D}_{\mathbf{q}}\right]\right)^{-1}\alpha^i, \tag{19}$$

$$\alpha^{i+1}=(\mathbf{I}+\Delta t\mathbf{A}_{\mathbf{x}})^{-1}\widetilde{\alpha}^i. \tag{20}$$

We note that $(\mathbf{I}+\Delta t\mathbf{A}_{\mathbf{x}})^{-1}$ is the same operator for all the components of α in configuration space and therefore it can be computed once and applied to all of them. On the other hand, although (19) is solved only in configuration space, the coefficients which multiply $\mathbf{B}_{\mathbf{q}}$, $\mathbf{C}_{\mathbf{q}}$ and $\mathbf{D}_{\mathbf{q}}$ vary in physical space. Furthermore, those coefficients change with time and so it is not possible to compute and store

$$\left(\mathbf{I}+\Delta t\left[\frac{\partial u_1}{\partial x_1}\mathbf{B}_{\mathbf{q}}+\frac{\partial u_1}{\partial x_2}\mathbf{C}_{\mathbf{q}}+\frac{\partial u_2}{\partial x_1}\mathbf{D}_{\mathbf{q}}\right]\right)^{-1}$$

once for all and a linear system should be solved at every grid point at each time-step. We will term the scheme (17) and (18) the "slow solver" in what follows. The following paragraph gives the outline of the fast solver.

As will be shown in the following subsections, one can construct a time discretization for the configurational part of the FP equation, which can be used instead of (17) and which can be written, after discretization, in the form

$$\widetilde{\alpha}^i=\mathbf{F}_{\mathbf{q}}(\mathbf{I}+k\Delta t\mathbf{E}_{\mathbf{q}})^{-1}\mathbf{G}_{\mathbf{q}}\alpha^i, \tag{21}$$

where the coefficient k varies in physical space and $\mathbf{E}_{\mathbf{q}}$ is a constant matrix. $\mathbf{F}_{\mathbf{q}}$ and $\mathbf{G}_{\mathbf{q}}$ are some matrices varying in physical space, but such that a matrix–vector product with them can be computed approximately with the same (or smaller) computational price as a matrix-vector product with a constant matrix. What is important here, is that instead of having three coefficients varying in physical space (namely $\partial u_1/\partial x_1$, $\partial u_1/\partial x_2$ and $\partial u_2/\partial x_1$), we now have only one (namely k), and this allows us to solve (21) efficiently. To see that, we diagonalize $\mathbf{E}_{\mathbf{q}}$; more specifically we call $\mathbf{D}$ the diagonal matrix formed with the eigenvalues of $\mathbf{E}_{\mathbf{q}}$. Then, there exists an invertible matrix $\mathbf{P}$ (formed by the eigenvectors of $\mathbf{E}_{\mathbf{q}}$) such that $\mathbf{E}_{\mathbf{q}}=\mathbf{P}\mathbf{D}\mathbf{P}^{-1}$ and we can rewrite (21) as

$$\widetilde{\alpha}^i=\mathbf{F}_{\mathbf{q}}(\mathbf{P}\mathbf{P}^{-1}+k\Delta t\mathbf{P}\mathbf{D}\mathbf{P}^{-1})^{-1}\mathbf{G}_{\mathbf{q}}\alpha^i=\mathbf{F}_{\mathbf{q}}\mathbf{P}(\mathbf{I}+k\Delta t\mathbf{D})^{-1}\mathbf{P}^{-1}\mathbf{G}_{\mathbf{q}}\alpha^i. \tag{22}$$

We can compute the matrices $\mathbf{P}$, $\mathbf{P}^{-1}$ and $\mathbf{D}$ once for all. Even if k varies in physical space, $(\mathbf{I}+k\Delta t\mathbf{D})$ is a diagonal matrix which is cheap to invert. Assume a size N for the matrices appearing in (19) or (22) and that these matrices are full. Solving (19) would require the solution of a linear system at each time-step and each grid point in physical space so the cost would be $\mathrm{O}(N^3)$ per time-step and grid point. On the other hand, $\widetilde{\alpha}^i$ obtained by (22) is the result of matrix–vector multiplication with $\mathbf{F}_{\mathbf{q}}\mathbf{P}$ and $\mathbf{P}^{-1}\mathbf{G}_{\mathbf{q}}$, so the cost would only be $\mathrm{O}(N^2)$ under the hypothesis on $\mathbf{F}_{\mathbf{q}}$ and $\mathbf{G}_{\mathbf{q}}$ mentioned above.

4.2. The Fokker–Planck equation in polar coordinates

The norm of the configuration vectors cannot exceed $\sqrt{b}$ for the FENE model, hence the pdf should be defined in the disc $|q|<\sqrt{b}$. Therefore, it seems natural to use polar coordinates (r,θ) to represent $\mathbf{q}$ as

$$q_1=r\cos\theta,\quad q_2=r\sin\theta\quad\text{with } r\in[0,\sqrt{b}[\text{ and }\theta\in[0,2\pi[. \tag{23}$$

We give now a detailed expression of (5) in variables (r,θ):

$$\frac{\partial\psi}{\partial t}+\mathbf{u}\cdot\nabla\psi=-rb_1(\boldsymbol{\kappa},\theta)\frac{\partial\psi}{\partial r}-b_2(\boldsymbol{\kappa},\theta)\frac{\partial\psi}{\partial\theta}+\frac{1}{2\lambda}\left(\frac{br}{b-r^2}+\frac{1}{r}\right)\frac{\partial\psi}{\partial r}+\frac{b^2}{\lambda(b-r^2)^2}\psi+\frac{1}{2\lambda}\frac{\partial^2\psi}{\partial r^2}+\frac{1}{2\lambda r^2}\frac{\partial^2\psi}{\partial\theta^2}, \tag{24}$$

where $\boldsymbol{\kappa}=\nabla\mathbf{u}$ and $b_1(\boldsymbol{\kappa},\theta)$ and $b_2(\boldsymbol{\kappa},\theta)$ are defined by

$$b_1(\boldsymbol{\kappa},\theta) = \kappa_{11}\cos 2\theta + \left(\frac{\kappa_{12}+\kappa_{21}}{2}\right)\sin 2\theta \tag{25}$$

and

$$b_2(\boldsymbol{\kappa},\theta) = -\kappa_{11}\sin 2\theta + \left(\frac{\kappa_{12}+\kappa_{21}}{2}\right)\cos 2\theta + \frac{\kappa_{21}-\kappa_{12}}{2}. \tag{26}$$

Eq. (24) should be supplied with the boundary conditions at $r = 0$ and $r = \sqrt{b}$. We take them into account by introducing a new unknown $\alpha(t,\mathbf{x},\eta,\theta)$ defined by

$$\psi(t,\mathbf{x},r,\theta) = \left(\frac{1-\eta}{2}\right)^2 \alpha(t,\mathbf{x},\eta,\theta), \tag{27}$$

where $r^2 = b((1+\eta)/2)$ and $\eta \in [-1,1]$. We require as well that $\alpha(t,\mathbf{x},\eta,\theta+\pi) = \alpha(t,\mathbf{x},\eta,\theta)$. Indeed, the change of independent variable from r to η and the restriction on the dependence on θ makes the function ψ symmetric with respect to $\mathbf{q}$. This is reasonable from the physical viewpoint (the two beads are indistinguishable) and implies the proper boundary condition $\partial\psi/\partial r = 0$ at $r = 0$ (or $\eta = -1$). The multiplier $((1-\eta)/2)^2 = (1-|\mathbf{q}|^2/b)^2$ is introduced into (27) to prevent the spring force (3) from becoming infinite for $r = \sqrt{b}$, (or $\eta = 1$). Although requiring that ψ vanishes at the boundary $r = \sqrt{b}$ seems the most natural thing to do, we have found experimentally that this boundary condition leads to numerical instabilities.

Substituting the expression for ψ given by (27) into (24), we get

$$\frac{\partial\alpha}{\partial t} + \mathbf{u}\cdot\nabla\alpha = b_1(\boldsymbol{\kappa},\theta)L_1\alpha - b_2(\boldsymbol{\kappa},\theta)\frac{\partial\alpha}{\partial\theta} + L_0\alpha, \tag{28}$$

where L_0 and L_1 are linear operators (independent of $\boldsymbol{\kappa}$) defined by

$$L_0\alpha = -\frac{4(b-4)\eta}{b\lambda(1-\eta)^2}\alpha + \left(\frac{2(b-8)(1+\eta)}{b\lambda(1-\eta)} + \frac{4}{b\lambda}\right)\frac{\partial\alpha}{\partial\eta} + \frac{4(1+\eta)}{\lambda b}\frac{\partial^2\alpha}{\partial\eta^2} + \frac{1}{\lambda b(1+\eta)}\frac{\partial^2\alpha}{\partial\theta^2} \tag{29}$$

and

$$L_1\alpha = 4\frac{1+\eta}{1-\eta}\alpha - 2(1+\eta)\frac{\partial\alpha}{\partial\eta}. \tag{30}$$

4.3. Time discretization of the Fokker–Planck equation

We are now in a position to construct a time marching scheme for the configurational part of the FP equation that we will use instead of (17) in our fast solver. It should be a first order approximation in time of the equation

$$\frac{\partial\alpha}{\partial t} = b_1(\boldsymbol{\kappa}^i,\theta)L_1\alpha - b_2(\boldsymbol{\kappa}^i,\theta)\frac{\partial\alpha}{\partial\theta} + L_0\alpha, \tag{31}$$

which is solved from $t = t_i$ to $t = t_{i+1}$, $\widetilde{\alpha}^i$ and α^i being set to $\alpha|_{t=t_{i+1}}$ and $\alpha|_{t=t_i}$, respectively. Introducing the following scalar functions

$$k(\boldsymbol{\kappa}) = \sqrt{\kappa_{11}^2 + (\kappa_{12}+\kappa_{21})^2/4}, \tag{32}$$

$$\varphi(\boldsymbol{\kappa}) = \frac{1}{2}\arctan\left(\frac{\kappa_{12}+\kappa_{21}}{2\kappa_{11}}\right) \tag{33}$$

and

$$k_a(\boldsymbol{\kappa}) = \frac{\kappa_{12} - \kappa_{21}}{2}, \tag{34}$$

we can rewrite (31) as

$$\frac{\partial \alpha}{\partial t} - k_a^i \frac{\partial \alpha}{\partial \theta} = -k^i \cos(2(\theta - \varphi^i)) L_1 \alpha + k^i \sin(2(\theta - \varphi^i)) \frac{\partial \alpha}{\partial \theta} + L_0 \alpha, \tag{35}$$

where the upper indices i were added to k, φ and k_a defined by (32)–(34) to emphasize the fact that those quantities are computed for the tensor $\boldsymbol{\kappa}^i$ that is updated at time $t = t_i$. In what follows, we denote explicitly the dependence of α on t and θ alone but it should be kept in mind that α is a function of η as well and that all the quantities (α, k, φ and k_a) depend on the position in physical space as a parameter.

We will use a time discretization of (35) of Crank–Nicolson type

$$\frac{\widetilde{\alpha}^i\left(\theta - \frac{1}{2} k_a^i \Delta t\right) - \alpha^i\left(\theta + \frac{1}{2} k_a^i \Delta t\right)}{\Delta t} = \mathrm{RHS}, \tag{36}$$

where

$$\begin{aligned} \mathrm{RHS} = & -\tfrac{1}{2} k^i \cos(2(\theta - \varphi^i)) L_1 \left(\widetilde{\alpha}^i(\theta - \tfrac{1}{2} k_a^i \Delta t) + \alpha^i(\theta + \tfrac{1}{2} k_a^i \Delta t)\right) \\ & + \tfrac{1}{2} k^i \sin(2(\theta - \varphi^i)) \left(\frac{\partial \widetilde{\alpha}^i}{\partial \theta}(\theta - \tfrac{1}{2} k_a^i \Delta t) + \frac{\partial \alpha^i}{\partial \theta}(\theta + \tfrac{1}{2} k_a^i \Delta t) \right) + \frac{1}{2} L_0 \left(\widetilde{\alpha}^i(\theta - \tfrac{1}{2} k_a^i \Delta t) + \alpha^i(\theta + \tfrac{1}{2} k_a^i \Delta t)\right). \end{aligned}$$

Appendix A provides a detailed derivation of (36). We note that this scheme would be a second order time accurate approximation of (35) if the velocity gradient were evaluated at time $t_{i+1/2}$. However this is not the case in view of the coupling with (18), and thus the resulting scheme (18)–(36) is only first order accurate in time. In the rest of this section, we shall show that (36) can be represented under the same form as (21), which enables us to apply the diagonalization technique outlined above.

Let Π_ϕ be the operator of rotation with the angle ϕ, which is defined for an arbitrary function $\Phi(\theta)$ by

$$\Pi_\phi \Phi(\theta) = \Phi(\theta + \phi). \tag{37}$$

Applying Π_{φ^i} to both sides of Eq. (36) and noting that Π_{φ^i} commutes with L_0, L_1 and $\partial/\partial\theta$, we get

$$\frac{\Pi_{\varphi^i - \frac{1}{2} k_a^i \Delta t} \widetilde{\alpha}^i(\theta) - \Pi_{\varphi^i + \frac{1}{2} k_a^i \Delta t} \alpha^i(\theta)}{\Delta t} = \Pi_{\varphi^i} \mathrm{RHS}, \tag{38}$$

where

$$\begin{aligned} \Pi_{\varphi^i} \mathrm{RHS} = & -\frac{1}{2} k^i \cos(2\theta) L_1 \left(\Pi_{\varphi^i - \frac{1}{2} k_a^i \Delta t} \widetilde{\alpha}(\theta) + \Pi_{\varphi^i + \frac{1}{2} k_a^i \Delta t} \alpha^i(\theta) \right) + \frac{1}{2} k^i \sin(2\theta) \frac{\partial}{\partial \theta} \left(\Pi_{\varphi^i - \frac{1}{2} k_a^i \Delta t} \widetilde{\alpha}(\theta) \right. \\ & \left. + \Pi_{\varphi^i + \frac{1}{2} k_a^i \Delta t} \alpha^i(\theta) \right) + \frac{1}{2} L_0 \left(\Pi_{\varphi^i - \frac{1}{2} k_a^i \Delta t} \widetilde{\alpha}(\theta) + \Pi_{\varphi^i + \frac{1}{2} k_a^i \Delta t} \alpha^i(\theta) \right). \end{aligned} \tag{39}$$

Let $\mathbf{M}_1$ be the matrix obtained by discretizing the operator

$$-\cos(2\theta) L_1 + \sin(2\theta) \frac{\partial}{\partial \theta}, \tag{40}$$

and $\mathbf{M}_0$ the matrix resulting from the discretization of the operator L_0. Then, (38) can be written in the discrete form as:

$$\frac{\Pi_{\varphi^i-\frac{1}{2}k_a^i\Delta t}\widetilde{\alpha}^i-\Pi_{\varphi^i+\frac{1}{2}k_a^i\Delta t}\alpha^i}{\Delta t}=\frac{1}{2}\mathbf{M}_0\left(\Pi_{\varphi^i-\frac{1}{2}k_a^i\Delta t}\widetilde{\alpha}^i+\Pi_{\varphi^i+\frac{1}{2}k_a^i\Delta t}\alpha^i\right)+\frac{k^i}{2}\mathbf{M}_1\left(\Pi_{\varphi^i-\frac{1}{2}k_a^i\Delta t}\widetilde{\alpha}^i+\Pi_{\varphi^i+\frac{1}{2}k_a^i\Delta t}\alpha^i\right), \tag{41}$$

where we have denoted the unknowns discretized in configuration space by the same symbols as the non-discretized ones. By rearranging (41) we get

$$\left(\frac{1}{\Delta t}\mathbf{I}-\frac{1}{2}\mathbf{M}_0-\frac{k^i}{2}\mathbf{M}_1\right)\Pi_{\varphi^i-\frac{1}{2}k_a^i\Delta t}\widetilde{\alpha}^i=\left(\frac{1}{\Delta t}\mathbf{I}+\frac{1}{2}\mathbf{M}_0+\frac{k^i}{2}\mathbf{M}_1\right)\Pi_{\varphi^i+\frac{1}{2}k_a^i\Delta t}\alpha^i \tag{42}$$

or

$$\widetilde{\alpha}^i=\Pi_{\frac{1}{2}k_a^i\Delta t-\varphi^i}\left(\mathbf{I}-k^i\Delta t\mathbf{E}_\mathbf{q}\right)^{-1}(\mathbf{R}+k^i\Delta t\mathbf{E}_\mathbf{q})\Pi_{\varphi^i+\frac{1}{2}k_a^i\Delta t}\alpha^i, \tag{43}$$

with the matrices $\mathbf{E_q}$ and $\mathbf{R}$ defined by

$$\mathbf{E}_\mathbf{q}=\frac{1}{2}\left(\mathbf{I}-\frac{\Delta t}{2}\mathbf{M}_0\right)^{-1}\mathbf{M}_1, \tag{44}$$

$$\mathbf{R}=\left(\mathbf{I}-\frac{\Delta t}{2}\mathbf{M}_0\right)^{-1}\left(\mathbf{I}+\frac{\Delta t}{2}\mathbf{M}_0\right). \tag{45}$$

We now recognize that (43) has the form of (21) and thus it can be solved efficiently using the diagonalization technique described in Section 4.1. In what follows we term the time splitting scheme consisting of (43) and (18) as the fast solver.

4.4. Discretization of the FP equation in configuration space

We shall search for an approximate solution $\alpha(t,\mathbf{x},\eta,\theta)$ to the FP equation (28) of the form

$$\alpha(t,\mathbf{x},\eta,\theta)=\sum_{i=0}^{1}\sum_{l=i}^{N_F}\sum_{k=1}^{N_R}\alpha_{kl}^i(t,\mathbf{x})h_k(\eta)\Phi_{il}(\theta) \tag{46}$$

with

$$\Phi_{il}(\theta)=(1-\mathrm{i})\cos(2l\theta)+\mathrm{i}\sin(2l\theta). \tag{47}$$

In the above expression, $\{h_k(\eta)\}_{1\leqslant k\leqslant N_R}$ are Lagrange interpolating polynomials based on the Gauss-Legendre points η_r (see the book of Canuto et al. [6] for more details) and have the property that $h_k(\eta_r)=\delta_{kr}\ k,r=1,\ldots,N_R$. Note that the set $\{\eta_r\}$ is chosen so that it does not include the points $\eta=-1$ and $\eta=1$ since the boundary conditions there are already taken into account by (27). Only the Fourier modes of even order are kept in (47) because of the symmetry of $\alpha(\eta,\theta)$. The integrals with respect to η are evaluated using the Gauss quadrature rule

$$\int_{-1}^{1}f(\eta)\,\mathrm{d}\eta\approx\sum_{i=1}^{N_R}\omega_i f(\eta_i), \tag{48}$$

where $\omega_i,\ 1\leqslant i\leqslant N_R$ is a unique set of positive numbers such that the integration rule is exact for all polynomials of degree $2N_R-1$ or less on the interval $[-1,1]$. The integrals with respect to θ can be computed analytically.

To calculate the components of the matrix $\mathbf{M}_0$ that is the discretization of the operator L_0 (29), we insert (46) into (29), form its product with a test function $h_m(\eta)\Phi_{jn}(\theta)$ and integrate over configuration space, to obtain

$$(\mathbf{M}_0)_{uv} = \delta_{ln}\left(\left(\frac{2(b-8)(1+\eta_m)}{b\lambda(1-\eta_m)} + \frac{4}{b\lambda}\right)h_k'(\eta_m) + \frac{4(1+\eta_m)}{\lambda b}h_k''(\eta_m) - \left(\frac{4\eta_m(b-4)}{b\lambda(1-\eta_m)^2} + \frac{4l^2}{\lambda b(1+\eta_m)}\right)\delta_{km}\right). \tag{49}$$

The mapping between the indices $u, v = 1, \ldots, N_R(2N_F+1)$ of the matrix $\mathbf{M}_0$ and i, j, k, l, m, n is $u = (m-1)(2N_F+1) + 2n - j + 1$ and $v = (k-1)(2N_F+1) + 2l - i + 1$ for $i, j = 0, 1$; $k, m = 1, \ldots, N_R$ and $l = i, \ldots, N_F$, $n = j, \ldots, N_F$.

Similarly, the discrete matrix $\mathbf{M}_1$, which is the discretization of (40), may be defined by

$$(\mathbf{M}_1)_{uv} = \left(2(1+\eta_m)h_k'(\eta_m) - 4\left(\frac{1+\eta_m}{1-\eta_m}\right)\delta_{km}\right)J_{iljn} + K_{iljn}\delta_{km}, \tag{50}$$

where

$$J_{iljn} = \frac{1}{\pi(1+\delta_{n0})}\int_0^{2\pi} \cos(2\theta)\Phi_{il}(\theta)\Phi_{jn}(\theta)\,\mathrm{d}\theta \tag{51}$$

and

$$K_{iljn} = \frac{1}{\pi(1+\delta_{n0})}\int_0^{2\pi} \sin(2\theta)\Phi_{il}'(\theta)\Phi_{jn}(\theta)\,\mathrm{d}\theta. \tag{52}$$

The rotation operator (37) is implemented by using the expression

$$\Pi_\phi \Phi_{il}(\theta) = \cos(2l\phi)\Phi_{il}(\theta) - (-1)^i \sin(2l\phi)\Phi_{il}(\theta). \tag{53}$$

4.5. Computation of the extra-stress

Having computed the pdf in $\mathbf{x}$ at time t, the extra-stress which will serve as a source term for the Stokes equations (1) and (2) might be written as (see Eq. (6))

$$\boldsymbol{\tau}(\mathbf{x}, t) = \frac{\eta_p}{\lambda}\left(\frac{b+4}{b}\right)\left(-\mathbf{I} + \int_{\mathrm{D}(0,\sqrt{b})} \mathbf{q}\otimes\mathbf{F}(\mathbf{q})\psi(t,\mathbf{x},\mathbf{q})\,\mathrm{d}\mathbf{q}\right). \tag{54}$$

Using (3) and (23), an expression for $\mathbf{q}\otimes\mathbf{F}(\mathbf{q})$ is

$$\mathbf{q}\otimes\mathbf{F}(\mathbf{q}) = \frac{r^2}{1-(r^2/b)}\mathbf{e}\otimes\mathbf{e} = b\left(\frac{1+\eta}{1-\eta}\right)\mathbf{e}\otimes\mathbf{e}, \tag{55}$$

where $\mathbf{e}$ is the unit vector $(\cos\theta, \sin\theta)$. With the help of (27), the integral appearing in (54) can now be rewritten as

$$\int_{D(0,\sqrt{b})} \mathbf{q}\otimes\mathbf{F}(\mathbf{q})\psi(t,\mathbf{x},\mathbf{q})\,\mathrm{d}\mathbf{q} = \int_{-1}^{1}\int_0^{2\pi} \frac{b^2}{32}(1-\eta^2)\alpha(t,\mathbf{x},\eta,\theta)\mathbf{e}\otimes\mathbf{e}\,\mathrm{d}\theta\,\mathrm{d}\eta. \tag{56}$$

We then replace $\alpha(t,\mathbf{x},\eta,\theta)$ in the above integral by its expression (46), evaluate the integral with respect to θ analytically and the integral with respect to η numerically. Most of the terms vanish and we get the following expressions for the three components of the extra-stress at each point $(t,\mathbf{x})$:

$$\tau_{xx} = \frac{\eta_p}{\lambda}\frac{b+4}{b}\left(-1+\frac{\pi b^2}{32}\sum_{i=1}^{N_R}\omega_i\left(1-\eta_i^2\right)\left(2\alpha_{i0}^0+\alpha_{i1}^0\right)\right), \tag{57}$$

$$\tau_{xy} = \frac{\eta_p}{\lambda}\frac{b+4}{b}\frac{\pi b^2}{32}\sum_{i=1}^{N_R}\omega_i\left(1-\eta_i^2\right)\alpha_{i1}^1, \tag{58}$$

$$\tau_{yy} = \frac{\eta_p}{\lambda}\frac{b+4}{b}\left(-1+\frac{\pi b^2}{32}\sum_{i=1}^{N_R}\omega_i\left(1-\eta_i^2\right)\left(2\alpha_{i0}^0-\alpha_{i1}^0\right)\right), \tag{59}$$

where ω_i are the quadrature weights.

In the following section, we will apply this new scheme for a well-known benchmark problem in non-Newtonian fluid mechanics and compare the results with the traditional stochastic Brownian simulations that was described in Section 3.

5. Numerical experiments

5.1. A benchmark problem

Numerical results for viscometric flows can be found in [7], so in the present paper we only report numerical results for a flow in a complex geometry. The problem of steady planar viscoelastic flow around a cylinder confined in a channel has become popular recently as evidenced by the numerous publications dealing with this benchmark problem and dating from the last three years or so (e.g. [9,10,12,21,23,26]). Despite the fact that there is no geometrical singularity, strong shear flows near solid walls and strong extensional flows in the wake of the cylinder make the numerical simulation a highly challenging task. We choose the aspect ratio $\Lambda = R/H = 1/2$, where H is the half width of the channel and R is the radius of the cylinder (see Fig. 2). The ratio of the solvent viscosity η_s to the total zero shear-rate viscosity $\eta = (\eta_p + \eta_s)$ was taken equal to 0.59 as is usually done by other authors, and the parameter b in (3) is taken equal to 20. A global Deborah number for this problem may be defined by

$$De = \frac{\lambda\overline{U}}{R}, \tag{60}$$

where $\overline{U}$ is the average velocity of the fluid in the channel at entry. The Deborah number measures the elasticity of the fluid and for non-trivial geometries, all numerical schemes break down at some point when the Deborah numbers is increased.

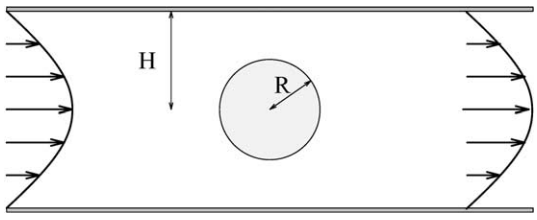

Fig. 2. Cylinder radius R placed symmetrically in a 2D channel of half width H.

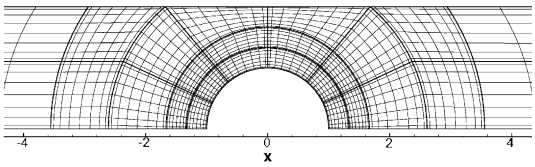

Fig. 3. Flow domain divided into 30 spectral elements for the level of discretization $N = 8$.

Periodic boundary conditions are used for the inflow and outflow of the channel for all quantities except the pressure which is periodic up to a linear function. The total length of the channel is 40 times the cylinder radius so that we can assume that the interaction of the cylinder with the other cylinders in the periodic array is negligible. We impose no-slip conditions on the cylinder surface and on the channel wall. In order to save in computational cost, we assume that the flow has $y = 0$ as a plane of symmetry so that only half of the domain needs to be considered. The problem is solved in this paper by dividing the flow domain into 30 conforming spectral elements and polynomial degrees ranging from $N = 8$ to $N = 10$ are used in the two spatial directions. A typical mesh is shown in Fig. 3 for $N = 8$ where the bold lines indicate the boundaries of the spectral elements and the intersections of the thin lines the position of the quadrature points. We use a SUPG spectral element-by-element method as described in [9] to solve the hyperbolic equations (10) and (18). The time-step Δt is chosen equal to 0.01. For the direct simulations based on the FP equation the iterations are stopped when the following convergence criterion is fulfilled for all collocation points $\mathbf{x} \in \Omega$:

$$\frac{|\mathbf{u}^{i+1}(\mathbf{x}) - \mathbf{u}^{i}(\mathbf{x})|}{\Delta t} \leqslant 10^{-4}. \tag{61}$$

It would be impossible to satisfy the same criterion with the stochastic simulations because of the presence of the random noise. The stochastic simulations are arbitrarily stopped instead at $t = 7$.

The most popular quantity used for the comparison of numerical results is the drag factor F^* on the cylinder:

$$F^* = \frac{F}{4\pi\eta\overline{U}}, \tag{62}$$

where F is the drag on the cylinder

$$F = \int_0^{\pi} \left\{ \left(-p + 2\eta_s \frac{\partial u_x}{\partial x} + \tau_{xx} \right) \cos\theta + \left(\eta_s \left(\frac{\partial u_y}{\partial x} + \frac{\partial u_x}{\partial y} \right) + \tau_{xy} \right) \sin\theta \right\} R \, \mathrm{d}\theta. \tag{63}$$

However, as noted in numerous papers ([2,8,11,12], for example), such a quantity is not a good indicator of the quality or accuracy of the solution. Therefore, we will not only give the value of the drag factor in this paper but we will also plot the tensile elastic normal stress in the wake of the cylinder, this being the most difficult flow region in which to resolve the solution convincingly.

5.2. Numerical results

5.2.1. Convergence with mesh refinement

Although the code did not blow up for Deborah numbers up to 1.5, it was only possible to prove convergence with mesh refinement up to $De = 1.2$. This is why we restrict ourselves to Deborah numbers less or equal to 1.2 in what follows. Proving convergence with mesh refinement for higher Deborah numbers would require exceedingly fine meshes.

We first demonstrate convergence with mesh refinement in both configuration and physical spaces for our highest Deborah number $De = 1.2$. This is done by plotting the xx-component of the extra-stress along the axis of symmetry ($|x/R| > 1$) and on the cylinder surface ($|x/R| \leqslant 1$) for the following two cases:

(1) The polynomial degree for the representation of the variables in physical space is kept at $N = 8$ and the resolution in configuration space is increased from $(N_F, N_R) = (10, 20)$ to $(N_F, N_R) = (12, 24)$.
(2) The resolution in configuration space is set at $(N_F, N_R) = (10, 20)$ and the polynomial degree in physical space is increased from $N = 8$ to $N = 10$.

Figs. 4 and 5 show that convergence with mesh refinement is achieved in both cases (1) and (2), respectively. Therefore, in the sequel we can restrict our numerical investigations by taking $(N_F, N_R, N) = (10, 20, 8)$.

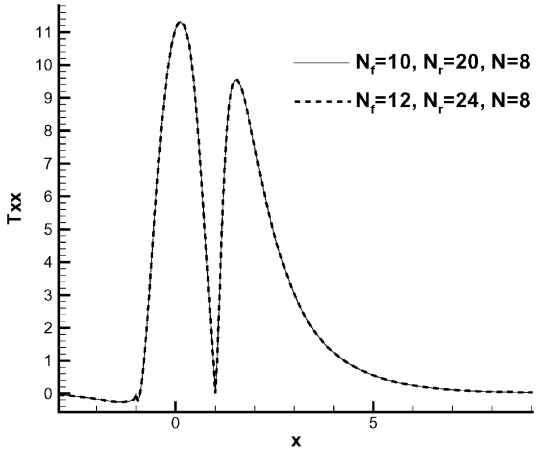

Fig. 4. xx-component of the extra-stress along the axis of symmetry and on the cylinder surface for $De = 1.2$ and two levels of discretization in configuration space.

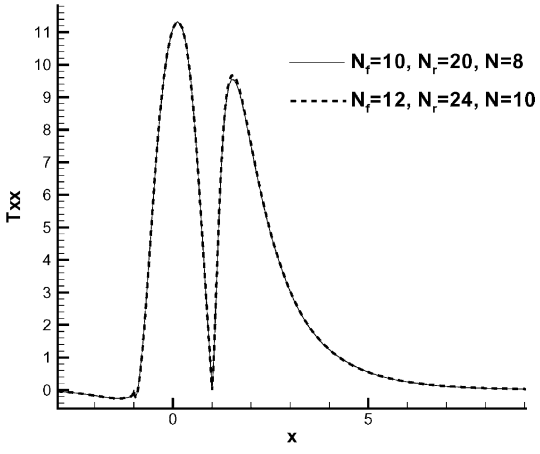

Fig. 5. xx-component of the extra-stress along the axis of symmetry and on the cylinder surface for $De = 1.2$ and two levels of discretization in physical space.

5.2.2. Comparison between direct simulations and stochastic simulations

We now compare the direct simulations with their stochastic equivalent in terms of accuracy and CPU cost. We first compare the drag factor as a function of time for the stochastic simulation when the number of realizations (M in Eq. (15)) is set to 1000 and then 16,000. The results are shown in Fig. 6 for a Deborah number $De = 0.8$ and clearly, the stochastic solution converges towards the solution of the direct approach as we increase the number of realizations. However for stochastic simulations, the rate of convergence is very low (typically $O(1/\sqrt{M})$). Note that for the two approaches, we have used the same resolution in physical space ($N = 8$). The same experiment is carried out in Fig. 7 but for a higher Deborah number ($De = 1.2$) and the conclusions remains unchanged.

Figs. 8 and 9 show the contour plots of the three components of the extra-stress (τ_{yy}, τ_{xy} and τ_{xx} from top to bottom) for the stochastic simulation (with 16,000 realizations) and the FP simulation, respectively, at a Deborah number $De = 1.2$. We can see that for the FP case, the three plots are reasonably smooth whereas for the stochastic case, wiggles appear in the plot of the xx-component of the extra-stress.

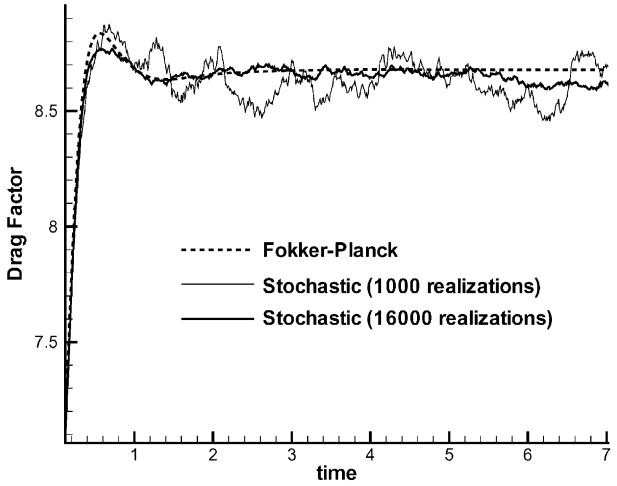

Fig. 6. Comparison of the drag factor for stochastic and direct simulations at $De = 0.8$.

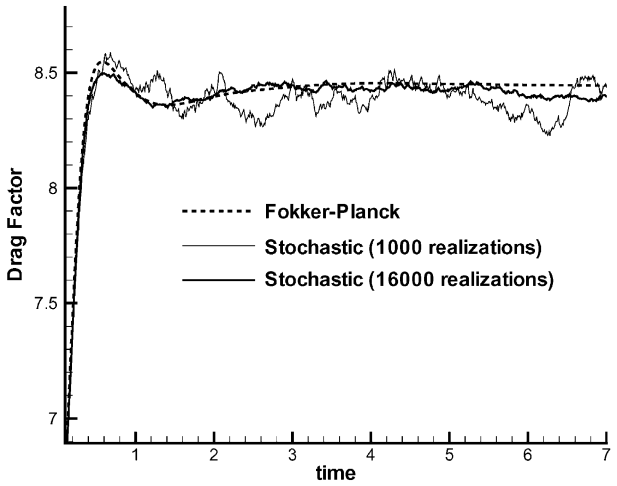

Fig. 7. Comparison of the drag factor for stochastic and direct simulations at $De = 1.2$.

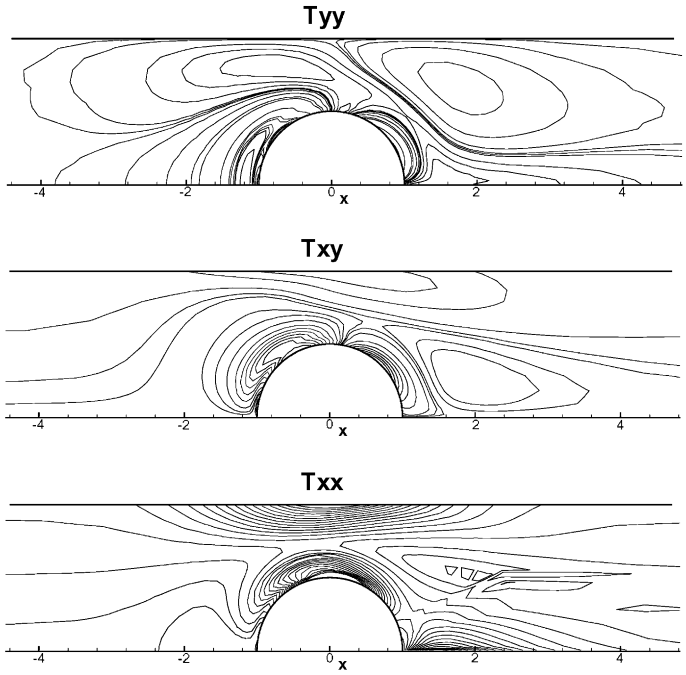

Fig. 8. Contour plot of the three components of the extra-stress. Stochastic simulation.

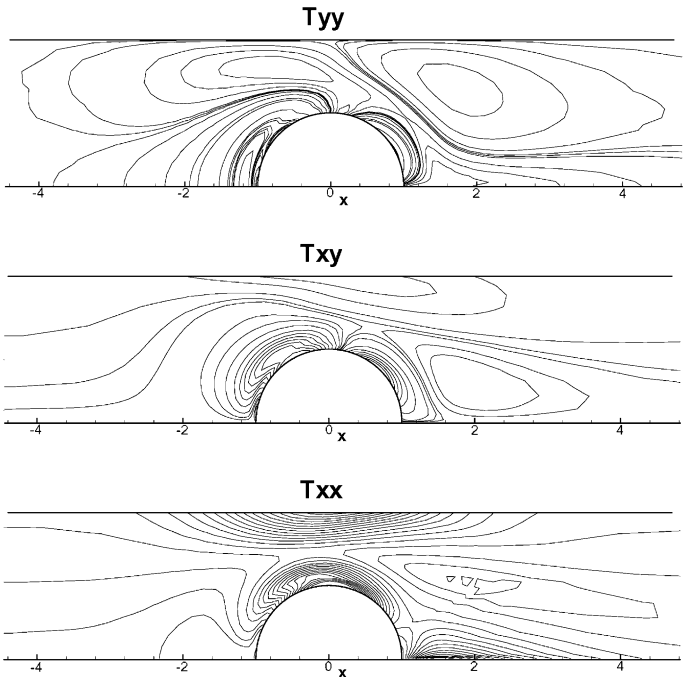

Fig. 9. Contour plot of the three components of the extra-stress. Direct simulation.

Table 1
Comparison of the CPU cost per time-step for the direct approach and for the stochastic approach

FP (fast solver)	FP (slow solver)	Stochastic – 1000	Stochastic – 16,000
3.3	198.0	18.0	285.0

Table 2
Drag factor F^* computed on uniform meshes ($N = 8, N_F = 10, N_R = 20$) for different Deborah numbers

De	0.6	0.7	0.8	0.9	1.0	1.1	1.2
Drag factor	8.8941	8.7729	8.6776	8.6008	8.5384	8.4865	8.4429

Fokker–Planck simulation.

We now turn our attention to the comparison of the CPU cost of the different approaches. Table 1 shows the average CPU time per time-step for the solution of the FP equation by the fast solver ()(18)–(43) with $(N_F, N_R, N) = (10, 20, 8)$, for the slow solver (17,18) with the same N_F, N_R and N and for the stochastic simulations (10) and (11) using 1000 and 16,000 realizations. Results are reported in seconds and the test was made on a PC with a Pentium IV 1.5 GHz processor. We see that the fast solver introduced in this paper produces a speedup of a factor 60 compared to the slow solver of [7]. The direct simulations using the fast solver are about 5.5 times faster than the stochastic simulation with a low number of realizations and up to 86 times faster for the case with 16,000 realizations. Because of the noise in the stochastic solution, in both cases, the direct approach is always more accurate.

Lastly we report in Table 2 the values of the drag factor on the cylinder as a function of the Deborah number for the direct simulation. To the author's knowledge, these values have not been available in the literature so far. The solutions of stochastic simulations are too noisy (see Figs. 6 and 7) to give an accurate average value of the drag factor.

6. Conclusions

In this paper, we have introduced a fast solver for the Fokker–Planck equation applied to viscoelastic flows calculations. The efficiency of the proposed solver was demonstrated by solving the benchmark problem of the flow around a cylinder constrained to lie between two parallel plates. Comparisons with traditional stochastic Brownian simulations for the 2D FENE model as well as our previous approach [7] have shown the advantages of this new method in terms of accuracy and efficiency. The ideas presented in this paper can be generalized to 3D FENE models and it is presently under investigation.

Acknowledgements

The authors thank Robert Owens for helpful discussions and for proofreading the manuscript. The work of the first author has been supported by the Swiss National Science Foundation, Grant Nos. 2100-55543 and 2100-57119.

Appendix A

In this appendix, we report the technical details which allow us to write (36). We assume that the function $\alpha(t, \theta)$ (the arguments $\mathbf{x}$ and η have been omitted for better clarity) is continuously differentiable with respect to t and θ so that using Taylor series around (t_i, θ), we have

$$\alpha(t_{i+\frac{1}{2}},\theta)=\alpha\left(t_i+\frac{\Delta t}{2},\theta\right)=\alpha(t_i,\theta)+\frac{\Delta t}{2}\frac{\partial\alpha}{\partial t}(t_i,\theta)+\mathrm{O}(\Delta t^2), \tag{A.1}$$

$$\alpha\left(t_i+\Delta t,\theta-\frac{1}{2}k_a^i\Delta t\right)=\alpha(t_i,\theta)+\Delta t\frac{\partial\alpha}{\partial t}(t_i,\theta)-\frac{1}{2}k_a^i\Delta t\frac{\partial\alpha}{\partial\theta}(t_i,\theta)+\mathrm{O}(\Delta t^2), \tag{A.2}$$

and

$$\alpha\left(t_i,\theta+\frac{1}{2}k_a^i\Delta t\right)=\alpha(t_i,\theta)+\frac{1}{2}k_a^i\Delta t\frac{\partial\alpha}{\partial\theta}(t_i,\theta)+\mathrm{O}(\Delta t^2). \tag{A.3}$$

We now subtract the half sum of the last two equations from the first one to obtain

$$\alpha(t_{i+\frac{1}{2}},\theta)=\frac{1}{2}\left(\alpha\left(t_{i+1},\theta-\frac{1}{2}k_a^i\Delta t\right)+\alpha\left(t_i,\theta+\frac{1}{2}k_a^i\Delta t\right)\right)+\mathrm{O}(\Delta t^2). \tag{A.4}$$

Differentiating this last equation with respect to θ, we also have

$$\frac{\partial\alpha}{\partial\theta}(t_{i+\frac{1}{2}},\theta)=\frac{1}{2}\left(\frac{\partial\alpha}{\partial\theta}\left(t_{i+1},\theta-\frac{1}{2}k_a^i\Delta t\right)+\frac{\partial\alpha}{\partial\theta}\left(t_i,\theta+\frac{1}{2}k_a^i\Delta t\right)\right)+\mathrm{O}(\Delta t^2). \tag{A.5}$$

Similarly we use Taylor series of the terms $\alpha(t_{i+1},\theta-\frac{1}{2}k_a^i\Delta t)$ and $\alpha(t_i,\theta+\frac{1}{2}k_a^i\Delta t)$ around the point $(t_{i+\frac{1}{2}},\theta)$ to obtain

$$\begin{aligned}\alpha\left(t_{i+1},\theta-\frac{1}{2}k_a^i\Delta t\right)&=\alpha\left(t_{i+\frac{1}{2}}+\frac{\Delta t}{2},\theta-\frac{1}{2}k_a^i\Delta t\right)\\&=\alpha(t_{i+\frac{1}{2}},\theta)+\frac{\Delta t}{2}\frac{\partial\alpha}{\partial t}(t_{i+\frac{1}{2}},\theta)-\frac{1}{2}k_a^i\Delta t\frac{\partial\alpha}{\partial\theta}(t_{i+\frac{1}{2}},\theta)+\mathrm{O}(\Delta t^2)\end{aligned} \tag{A.6}$$

and

$$\begin{aligned}\alpha\left(t_i,\theta+\frac{1}{2}k_a^i\Delta t\right)&=\alpha\left(t_{i+\frac{1}{2}}-\frac{\Delta t}{2},\theta+\frac{1}{2}k_a^i\Delta t\right)\\&=\alpha(t_{i+\frac{1}{2}},\theta)-\frac{\Delta t}{2}\frac{\partial\alpha}{\partial t}(t_{i+\frac{1}{2}},\theta)+\frac{1}{2}k_a^i\Delta t\frac{\partial\alpha}{\partial\theta}(t_{i+\frac{1}{2}},\theta)+\mathrm{O}(\Delta t^2).\end{aligned} \tag{A.7}$$

Subtracting (A.6) from (A.7) and dividing by Δt gives

$$\frac{\partial\alpha}{\partial t}(t_{i+\frac{1}{2}},\theta)-k_a^i\frac{\partial\alpha}{\partial\theta}(t_{i+1/2},\theta)=\frac{\alpha\left(t_{i+1},\theta-\frac{1}{2}k_a^i\Delta t\right)-\alpha\left(t_i,\theta+\frac{1}{2}k_a^i\Delta t\right)}{\Delta t}+\mathrm{O}(\Delta t). \tag{A.8}$$

We now evaluate (35) at $t=t_{i+\frac{1}{2}}$, use the relations (A.4), (A.5), (A.8), neglect the terms of order $\mathrm{O}(\Delta t)$ and denote similarly to (17) $\widetilde{\alpha}^i(\theta)=\alpha(t_{i+1},\theta)$ and $\alpha^i=\alpha(t_i,\theta)$ to get (36).

References

[1] R.C. Armstrong, R. Nayak, R.A. Brown, The use of kinetic theory and microstructural models in the analysis of complex flows of viscoelastic liquids, in: Aït-Kadi, J.M. Dealy, D.F. James, M.C. Williams (Eds.), Proceedings of the 12th International Congress on Rheology, Laval University, Québec, August 18–23, 1996.

[2] F.P.T. Baaijens, S.H.A. Selen, H.P.W. Baaijens, G.W.M. Peters, H.E.H. Meijer, Viscoelastic flow past a confined cylinder of a low density polyethylene melt, J. Non-Newtonian Fluid Mech. 68 (1997) 173–203.

[3] R.B. Bird, R.C. Armstrong, O. Hassager, Dynamics of Polymeric Liquids, vol. 2, Kinetic Theory, second ed., Wiley-Interscience, New York, Chichester, Brisbane, Toronto, Singapore, 1987.
[4] J. Bonvin, Numerical simulation of viscoelastic fluids with mesoscopic models, Ph.D. Thesis, École Polytechnique F édérale de Lausanne, Lausanne, Switzerland, 2000.
[5] J. Bonvin, M. Picasso, Variance reduction methods for CONNFFESSIT-like simulations, J. Non-Newtonian Fluid Mech. 84 (1999) 191–215.
[6] C. Canuto, M.Y. Hussaini, A. Quarteroni, T.A. Zang, Spectral Methods in Fluid Dynamics, Springer, Berlin, Heidelberg, 1988.
[7] C. Chauviere, A. Lozinski, Simulation of dilute polymer solutions using a Fokker–Planck equation, Comput. Fluids, to appear.
[8] C. Chauviere, R.G. Owens, How accurate is your solution? Error indicators for viscoelastic flow calculations, J. Non-Newtonian Fluid Mech. 95 (2000) 1–33.
[9] C. Chauvière, R.G. Owens, A new spectral element method for the reliable computation of viscoelastic flow, Comput. Methods Appl. Mech. Engrg. 90 (2001) 3999–4018.
[10] H.S. Dou, N. Phan-Thien, The flow of an Oldroyd-B fluid past a cylinder in a channel: adaptive viscosity vorticity (DAVSS-ω) formulation, J. Non-Newtonian Fluid Mech. 87 (1999) 47–73.
[11] Y.R. Fan, A comparative study of the discontinuous Galerkin and continuous SUPG finite element methods for computation of viscoelastic flows, Comput. Methods Appl. Mech. Engrg. 141 (1997) 47–65.
[12] Y.R. Fan, R.I. Tanner, N. Phan-Thien, Galerkin/least-squares finite-element methods for steady viscoelastic flows, J. Non-Newtonian Fluid Mech. 84 (1999) 233–256.
[13] X.-J. Fan, Viscosity, first normal-stress coefficient, and molecular stretching in dilute polymer solutions, J. Non-Newtonian Fluid Mech. 17 (1985) 125–144.
[14] X. Fan, Molecular models and flow calculation: I. The numerical solutions to multibead-rod models in inhomogeneous flows, Acta Mech. Sin. 5 (1989) 49–59.
[15] X. Fan, Molecular models and flow calculations: II. Simulation of steady planar flow, Acta Mech. Sin. 5 (1989) 216–226.
[16] D.J. Hingham, An algorithmic introduction to numerical simulation of stochastic differential equations, SIAM Rev. 43 (2001) 525–546.
[17] M.A. Hulsen, A.P.G. van Heel, B.H.A.A. van den Brule, Simulation of viscoelastic flows using Brownian configuration fields, J. Non-Newtonian Fluid Mech. 70 (1997) 79–101.
[18] A. Lozinski, C. Chauvière, J. Fang, R.G. Owens, A Fokker–Planck simulation of fast flows of concentrated polymer solutions in complex geometries, J. Rheol. 47 (2003) 535–561.
[19] R. Nayak, Molecular simulation of liquid crystal polymer flow: a wavelet-finite element analysis, Ph.D. Thesis, MIT, Cambridge, MA., 1998, p. 374.
[20] H.C. Öttinger, Stochastic processes in polymeric fluids, Springer, Berlin, 1996.
[21] R.G. Owens, C. Chauvière, T.N. Phillips, A locally upwinded spectral technique (LUST) for viscoelastic flows, J. Non-Newtonian Fluid Mech. 108 (2002) 49–72.
[22] R.G. Owens, T.N. Phillips, Computational Rheology, Imperial College Press/World Scientific, Singapore, 2002.
[23] N. Phan-Thien, H.-S. Dou, Viscoelastic flow past a cylinder: drag coefficient, Comput. Methods Appl. Mech. Engrg. 180 (1999) 243–266.
[24] R. Sizaire, G. Lielens, I. Jaumain, R. Keunings, V. Legat, On the hysteretic behaviour of dilute polymer solutions in relaxation following extensional flow, J. Non-Newtonian Fluid Mech. 82 (1999) 233–253.
[25] J.K.C. Suen, Y.L. Joo, R.C. Armstrong, Molecular orientation effects in viscoelasticity, Annu. Rev. Fluid Mech. 34 (2002) 417–444.
[26] J. Sun, M.D. Smith, R.C. Armstrong, R.A. Brown, Finite element method for viscoelastic flows based on the discrete adaptive viscoelastic stress splitting and the discontinuous Galerkin method: DAVSS-G/DG, J. Non-Newtonian Fluid Mech. 86 (1999) 281–307.
[27] A.P.G. van Heel, M.A. Hulsen, B.H.A.A. van den Brule, On the selection of parameters in the FENE-P model, J. Non-Newtonian Fluid Mech. 75 (1998) 253–271.
[28] H.R. Warner, Kinetic theory and rheology of dilute suspensions of finitely extensible dumbbells, Ind. Eng. Chem. Fundam. 11 (1972) 379–387.